COUPLING MARS' DUST AND WATER CYCLES: EFFECTS ON DUST LIFTING VIGOR, SPATIAL EXTENT AND SEASONALITY.

M. A. Kahre, *Bay Area Environmental Research Institute / NASA Ames Research Center, Moffett Field, CA, USA. (melinda.a.kahre@nasa.gov),* **J. L. Hollingsworth, R. M. Haberle,** *NASA Ames Research Center, Moffett Field, CA, USA.* **F. Montmessin,** *Laboratoire Atmosphères, Milieux, Observations Spatiales, France***,**

Introduction: The dust cycle is an important component of Mars' current climate system. Airborne dust affects the radiative balance of the atmosphere, thus greatly influencing the thermal and dynamical state of the atmosphere. Dust raising events on Mars occur at spatial scales ranging from meters to planet-wide. Although the occurrence and season of large regional and global dust storms are highly variable from one year to the next, there are many features of the dust cycle that occur year after year. Generally, a low-level dust haze is maintained during northern spring and summer, while elevated levels of atmospheric dust occur during northern autumn and winter. During years without global-scale dust storms, two peaks in total dust loading were observed by MGS/TES: one peak occurred before northern winter solstice at L_s 200-240, and one peak occurred after northern winter solstice at L_s 305-340 (Smith, 2004). These maxima in dust loading are thought to be associated with transient eddy activity in the northern hemisphere, which has been observed to maximize pre- and post-solstice (Barnes, 2003; Banfield et al., 2004, Wang, 2007).

Interactive dust cycle studies with Mars General Circulation Models (MGCMs) have included the lifting, transport, and sedimentation of radiatively active dust. Although the predicted global dust loadings from these simulations capture some aspects of the observed dust cycle, there are marked differences between the simulated and observed dust cycles (Kahre et al., 2006; Basu et al., 2004; Newman et al., 2002). Most notably, the maximum dust loading is robustly predicted by models to occur near northern winter solstice and is due to dust lifting associated with down slope flows on the flanks of the Hellas basin. Thus far, models have had difficulty simulating the observed pre- and post- solstice peaks in dust loading.

Interactive dust cycle studies typically have not included the formation of water ice clouds or their radiative effects. Water ice clouds can influence the dust cycle by scavenging dust from atmosphere and by interacting with solar and infrared radiation, thereby modifying the thermal structure of the atmosphere and its circulation. Results presented in other papers at this workshop show that including the radiative effects of water ice clouds greatly influence the water cycle (Haberle et al., 2011) and the vigor of weather systems in both the northern and southern hemispheres (Hollingsworth et al., 2011).

Our goal is to investigate the effects of fully coupling the dust and water cycles on the dust cycle. We show that including water ice clouds and their radiative effects greatly affect the magnitude, spatial extent and seasonality of dust lifting and the season of maximum atmospheric dust loading.

Methods: We use the NASA Ames Mars GCM (version 2.1d) for this investigation. This version of the model runs with a horizontal resolution of 5° in latitude by 6° in longitude. The vertical sigma-coordinate grid contains 24 layers and extends to approximately 80 km. This version of the model includes a 2-stream radiative transfer scheme that accounts for gaseous absorption and scattering aerosols and a tracer transport scheme based on the Van Leer formulation. A fully interactive dust cycle is implemented, which includes the lifting, transport and removal of radiatively active dust (Kahre et al., 2006, 2008). Dust is lifted from the surface when the momentum imparted to the surface (characterized as the surface wind stress, τ) exceeds a critical value, $\tau^* = 22.5$ mN m^{-2}. Lifted dust is partitioned into a lognormal distribution with an effective radius of 2.5 μm and an effective variance of 0.5. Airborne dust interacts with solar and infrared radiation, provides seed nuclei for water ice clouds, and undergoes gravitational sedimentation as free dust and as cores of water ice cloud particles. A complete water cycle is included that contains sublimation from the north residual cap and the microphysical processes of nucleation, growth, and settling of water ice clouds (Montmessin et al., 2002, 2004). Water ice clouds can either be radiatively active or inert.

Simulations: Three model simulations were carried out for this investigation (Table 1). These simulations were designed to explore the sensitivity of the dust cycle to the inclusion of cloud formation and the radiative effects of clouds.

Table 1:

Run I.D.	Interactive Dust?	Clouds?	Radiatively Active Clouds?
No Clouds	Yes	No	N/A
Clouds	Yes	Yes	No
R. A. Clouds	Yes	Yes	Yes

Results: Simulated results indicate that including the couplings between the dust and water cycles greatly affect the predicted dust cycle.

Annual Dust Cycle: The annual global dust opacity for the three simulated cases are shown in Figure 1. The simulations without clouds and with radiatively inert clouds produce similar dust cycles; these simulations closely resemble previous interactive dust cycle simulations that included wind stress dust lifting only. The global dust opacity during northern spring and summer is low compared to observations. The simulation that included inert clouds predicts a lower-level dust loading during these seasons due to the scavenging of dust by clouds. In previous studies, a parameterization for dust devil lifting has been included to provide a background dust haze during these seasons (Kahre et al., 2006). A peak in global dust opacity occurs near winter solstice and is due in large part to lifting along the north and south flanks of Hellas (Figure 2 top and middle panels). The inclusion of inert clouds slightly increases the vigor of dust raising events near the north growing and south receding seasonal CO_2 caps at L_s 200-240 and reduces dust lifting in the Hellas region at L_s~270.

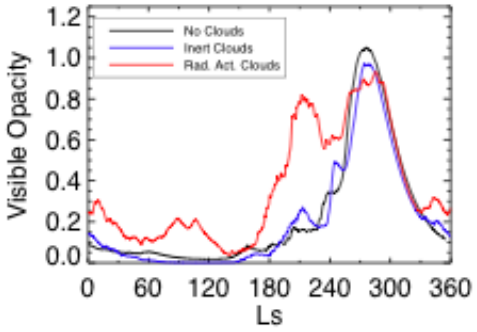

Figure 1: Globally averaged dust opacity for the three simulations discussed.

The radiative effects of clouds have a profound effect on the simulated dust cycle (Figure 1 and Figure 2 bottom panel). An increased level of dustiness is maintained throughout northern spring and summer, caused by wind stress lifting along the receding north seasonal cap and in the tropics. During northern autumn and winter, the global dust loading exhibits two distinct maxima, one centered at Ls~210 and one centered at Ls~270. Rigorous wind stress lifting at high northern latitudes before the north seasonal CO_2 cap starts to grow and along the south receding seasonal CO_2 cap causes the pre-solstice peak.

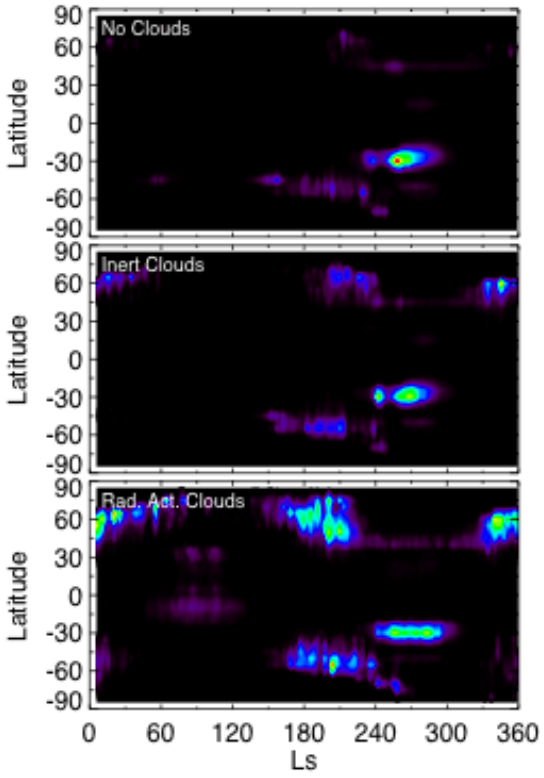

Figure 2: Zonally averaged wind stress dust lifting rate for the three simulations.

Atmospheric Thermal Structure at L_s 210. Atmospheric temperatures at L_s 210 exhibit differences between the three simulations (Figure 3). Although radiatively inert clouds do not directly affect atmospheric heating rates, they influence the thermal structure of the atmosphere (and therefore the circulation and lifting potential of the atmosphere) by modifying the vertical distribution of dust through scavenging. The presence of radiatively inert clouds results in warmer temperatures throughout the atmosphere as compared to the no cloud case (Figure 3 top and middle panels). This might be counterintuitive because one would expect clouds to confine dust near to the surface resulting in cooler air aloft. In this case, the atmosphere is warmed in the presence of inert clouds because dust lifting is more vigorous so the atmosphere is dustier at this season (see Figure 1 blue and black curves).

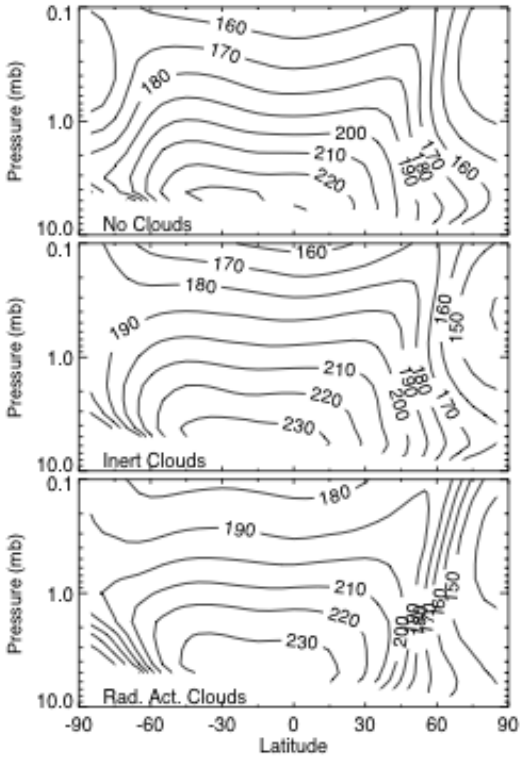

Figure 3: Zonally averaged atmospheric temperatures at L_s 210 for the three simulations.

Compared to the other two cases, when the radiative effects of water ice clouds are included the predicted temperatures agree better with observations. The atmosphere is warmer in the tropics but cooler near the surface in the polar regions. These effects are due to a combination of the direct radiative effects of clouds and the increased dust loading that is present in this simulation (see Figure 1 red curve). The combined effect of warming at low latitudes and cooling at high latitudes is to make the atmosphere in the middle northern latitudes more isothermal and to tighten the equator-to-pole thermal gradient (i.e., the baroclinicity of the atmosphere). The increased baroclinicity supports more rigorous transient eddies (see Hollingsworth et al. 2011, this workshop), which most likely causes the increase in the vigor of dust lifting at high northern latitudes that produces the global opacity peak at this pre-solstice season.

Spatial Extent of Dust Lifting at L_s 210. The spatial extent of dust source regions at this season is also sensitive to the couplings between the dust and water cycle (Figure 4). Compared to the no cloud case, including radiatively inert clouds expands the longitudinal extent of dust lifting in the northern middle to high latitudes. When the radiative effects of clouds are included, the dust lifting is predicted throughout nearly all longitudes polewards of 30 N in the northern hemisphere. This longitudinally broad band of dust lifting is the most consistent with the patterns of dust injection predicted by MGCM simulations that utilize assimilation methods for the treatment of dust lifting (Kahre et al., 2009).

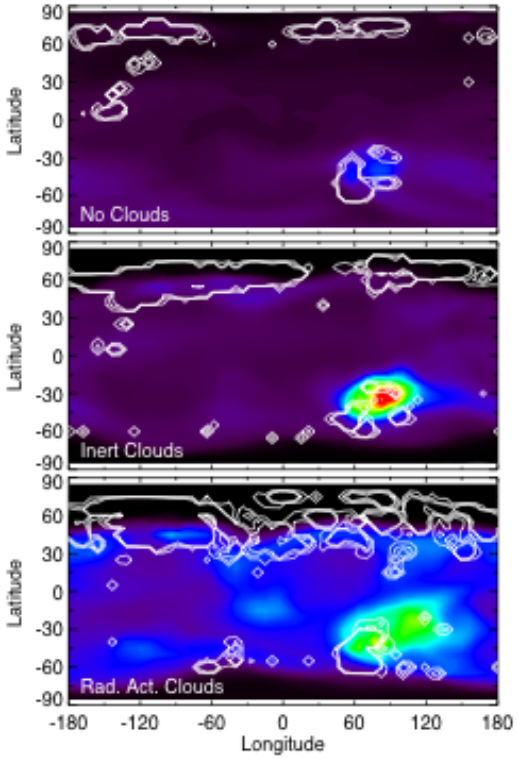

Figure 4: Column dust opacity (fill) and dust lifting rate (contours) at L_s 210 for the three simulations

Discussion and Conclusions: Preliminary fully coupled dust and water cycle simulations show improvements in some aspects of the simulated dust cycle. Most interestingly, increased eddy activity at L_s 180-240 increases the vigor and spatial extent of dust lifting in the northern hemisphere. This increased dust lifting produces a peak in global opacity at a season that is more consistent with TES observations during non-global dust storm years than the simulations that do not include clouds and their radiative effects. Additionally, the spatial extent of dust lifting when the radiative effects of clouds are included is expanded, which is in better agreement to dust assimilation simulations and MGS/MOC observations of dust events. Because of the effects of coupling the dust and water cycles discussed here, it is very likely that these couplings are vital to the simulation of the dust cycle.

Although improvements to the simulated dust cycle are seen in these coupled simulations, it is apparent that there is much work that still needs to be done to get both the dust and water cycles 'right'. Dust lifting in the Hellas region during northern win-

ter is over-predicted. Limiting the supply of dust in these regions may be appropriate. More troubling is the effect of coupling the dust and water cycles through cloud formation on the individual water and CO_2 cycles. The simulated spatial and temporal patterns of atmospheric water vapor and water ice clouds do not agree well with observations. The presence of large quantities of radiatively active dust at high northern latitudes during northern autumn slows the growth of the north seasonal CO2 cap. The resulting pressure cycle at the Viking Lander sites are out of phase compared to observations. It is clear that a full understanding of the interactions between the three climate cycles will be required for an understanding of each individually.

References:

Banfield, D., M.J. Conrath, P.J. Gierasch, R.J. Wilson, and M.D. Smith (2004), Travelind waves in the Martian atmosphere from MGS TES Nadir data. *Icarus*, **161**, 319-345.

Barnes, J.R. (2003), Planetary eddies in the Martian atmosphere: FFSM analysis of TES data. *Mars Atmosphere Modeling and Observations Workshop*, Granada, Spain, 13-15 January.

Basu, S. and M.I. Richardson (2004), Simulation of the Martian dust cycle with the GFDL Mars GCM. *JGR* **109**(46), 11006.

Cantor, B.A., P.B. James, M. Caplinger, and M.J. Wolff (2001), Martian dust storms: 1999 Mars Orbiter Camera observations. *JGR*, **106**, 23653-23687.

Haberle, R.M., F. Montmessin, M.A. Kahre, J.L. Hollingsworth, J. Schaeffer, M.J. Wolff, and R.J. Wilson (2011), Radiative effects of water ice clouds on the Martian seasonal water cycle. *Fourth International Workshop on the Mars Atmosphere: Modeling and Observations*, Paris, France, 8-11 February.

Hollingsworth, J.L., M.A. Kahre, R.M. Haberle, and F. Montmessin (2011), Radiatively-active aerosols within Mars' atmosphere: Implications on the weather and climate as simulated by the NASA ARC Mars GCM. *Fourth International Workshop on the Mars Atmosphere: Modeling and Observations*, Paris, France, 8-11 February.

Kahre, M.A., J.R. Murphy, and R.M. Haberle (2006), Modeling the Martian dust cycle and surface dust reservoirs with the NASA Ames General Circulation Model. *JGR*, **111**(E6).

Kahre, M.A., R.J. Wilson, R.M. Haberle, and J.L. Hollingsworth (2009), An inverse approach to modeling the dust cycle with two Mars General Circulation Models. *Mars Dust Cycle Workshop*, Moffett Field, CA.

Montmessin, F., P. Rannou, and M. Cabane (2002), New insights into Martian dust distribution and water-ice cloud microphysics. *JGR*, **107**, 5037.

Montmessin, F., F. Forget, P. Rannou, M. Cabane, and R. M. Haberle (2004), Origin and role of water ice clouds in the Martian water cycle as inferred from a general circulation model. *JGR*, **109**, 10004.

Newman, C.E., S.R. Lewis, P.L. Read, and F. Forget (2002), Modeling the Martian dust cycle-2. Multiannual radiatively active dust transport simulations. *JGR*, **107**, 5124.

Smith, M.D. (2004), Interannual variability in TES atmospheric observations of Mars dust 1999-2003 *Icarus*, **167**(1), 148-165.

Wang, H. (2007), Dust storms originating in the northern hemisphere during the third mapping year of Mars Global Surveyor. *Icarus*, **189**, 325-343.